A comparison of multicomponent electrosorption in capacitive deionization and membrane capacitive deionization

Armineh Hassanvand[a], George Q. Chen[a,b], Paul A. Webley[a], Sandra E. Kentish[a,b,*]

[a] School of Chemical and Biomedical Engineering, University of Melbourne, Parkville, VIC 3010, Australia

[b] The ARC Dairy Innovation Hub, Department of Chemical Engineering, University of Melbourne, Parkville, VIC 3010, Australia

*Corresponding Author:

E-mail address: sandraek@unimelb.edu.au (S.E.Kentish).

Postal address: School of Chemical and Biomedical Engineering, The University of Melbourne, Parkville, 3010 Victoria, Australia

Tel.: +61 3 83446682.

Abstract

In this study, the desalination performance of Capacitive Deionization (CDI) and Membrane Capacitive Deionization (MCDI) was studied for a wide range of salt compositions. The comprehensive data collection for monovalent and divalent ions used in this work enabled us to understand better the competitive electrosorption of these ions both with and without ion-exchange membranes (IEMs). As expected, MCDI showed an enhanced salt adsorption and charge efficiency in comparison with CDI. However, the different electrosorption behavior of the former reveals that ion transport through the IEMs is a significant rate-controlling step in the desalination process. A sharper desorption peak is observed for divalent ions in MCDI, which can be attributed to a portion of these ions being temporarily stored within the IEMs, thus they are the first to leave the cell upon discharge. In addition to salt concentration, we monitored the pH of the effluent stream in CDI and MCDI and discuss the potential causes of these fluctuations. The dramatic pH change over one adsorption and desorption cycle in CDI (pH range of 3.5 to 10.5) can be problematic in a feed water containing components prone to scaling. The pH change, however, was much more limited in the case of MCDI for all salts.

Keywords: capacitive deionization; electrosorption; desalination; sulfate; nitrate; calcium.

Introduction

The shortage of fresh water has become a severe problem in our time owing to population and economic growth, as well as the impacts of climate change. This has made desalination of sea and brackish water stand out as an increasingly necessary answer to resolve the water crisis. Among desalination technologies, capacitive deionization (CDI) has attracted attention as an energy-efficient and promising electrochemical desalination technology, especially for low salinity brackish water (Bouhadana et al. 2010, Subramani and Jacangelo 2015). In the most common approach to CDI, the influent stream passes between two high-capacitance electrodes made of porous carbon materials to which an electrical voltage or current is applied. As a result, anions and cations are temporarily stored on the porous surface of the oppositely charged electrode and a deionized stream with lower ion concentration flows out of the cell. Ion electrosorption is based on the formation of electrical double layers (EDLs) inside the micropores (< 2 nm) of the electrodes (Porada et al. 2013). After a period of operation, the electrodes become saturated and require regeneration. In this step, the cell voltage or current is reduced to zero and adsorbed ions are released into a wastewater stream. To summarize, a CDI cycle consists of two steps, ion adsorption and ion desorption. While CDI is only economic for relatively dilute solutions, it has low energy consumption as it removes ions from the electrolyte rather than separating water from the salty stream, such as in reverse osmosis and distillation (Asquith et al. 2015, Liu et al. 2015).

To improve performance, ion-exchange membranes (IEMs) can be placed in front of the electrodes. This approach, which is one of the most recent developments in CDI, is called Membrane Capacitive Deionization (MCDI) (Biesheuvel and van der Wal 2010). In this case, cation and anion exchange membranes placed in front of the negatively and positively charged electrodes, respectively, will only allow counter-ions to move from the bulk solution toward the electrode. By blocking almost all of co-ions, the desalination process is more efficient as

there is less co-ion repulsion. Furthermore, the use of IEMs enables us to reverse the polarity of the cell during desorption, which leads to a more complete expulsion of counter-ions from the micro and macropores of the carbon (Zhao et al. 2012a). In addition to the favorable features of CDI including low energy consumption, easy regeneration and maintenance (Wang et al. 2015), MCDI operation is more stable which makes this technique an attractive water treatment technology for industrial applications (Kim et al. 2010). Biesheuvel et al. (Biesheuvel et al. 2011), Zhao et al. (Zhao et al. 2012a) and Dykstra et al. (Dykstra et al. 2016a) have presented comprehensive ion transport models for desalination using MCDI.

Ion charge and size plays an important role, given that the CDI process is based on temporary adsorption of ions inside the EDLs of the carbon micropores. However, few studies on CDI performance have focused on salts other than NaCl. Pioneers of this work were Gabelich et al. (Gabelich et al. 2002) who investigated the sorption capacity of carbon aerogel electrodes for various monovalent and divalent ions. They reported that monovalents are preferentially removed over divalent ions due to smaller hydrated radii. Zhao et al. (Zhao et al. 2012b) similarly observed preferential adsorption of Na^+ over Ca^{2+}; however, they reported Na^+ replacement with Ca^{2+} later during adsorption. In contrast, Xu et al. (Xu et al. 2008) and Mossad et al. (Mossad et al. 2013, Mossad and Zou 2012) recognized ionic charge as the factor controlling the electrosorption preference in a competitive environment. It is worth mentioning that the last three research groups studied the CDI performance with an electrolyte consisting of non-equal concentration of ions. In other words, as the ion concentration is one of the variables influencing the removal rate of that specific ion, it is questionable to attribute the preferential electrosorption sequence reported by them to ionic charge alone. A few studies have investigated the effect of ion properties on electrosorption while keeping the concentration equal for different salts. Seo et al. (Seo et al. 2010) reported selective ion removal for a mixture of cations including sodium, potassium, magnesium and calcium at different flow

rates. They attributed the adsorption sequence to the pore size and structure of the carbon material. In another work, Huyskens et al. (Huyskens et al. 2013) measured the ion removal for various monovalent and divalent salts; however, their result was not in agreement with that of Seo et al (Seo et al. 2010). Later, Han et al. (Han et al. 2014), in a comprehensive data collection on removal of various monovalent ions in CDI using different activated carbon cloths, showed that sorption capacity and competitive ion removal can be tuned by varying the accessible surface area of carbon and its micro to meso-porosity ratio. Discrepancies between these reports indicate that more research is needed to fully understand the competitive electrosorption of different ions, especially in the presence of divalent ions. In the area of EDL modelling, (Suss 2017) extended the existing models by accounting for ion volume exclusion interactions to demonstrate selective ion removal based on ion size.

The focus in MCDI has predominantly been on the removal of different salts using novel electrodes or IEMs (Kim et al. 2016, Kim and Choi 2012). However, very few research groups have compared the removal rate of different ions in MCDI using commercially available IEMs. In 2012, Kim et al. (Kim et al. 2013) manipulated the removal of chloride and nitrate in single and mixed solutions by varying the current density in MCDI. In a recent publication, Tang et al. (Tang et al. 2017b) studied the removal of sulfate in MCDI and observed more sulfate removal in a mixture of sulfate and chloride with equal molar concentrations. As diffusion of the ions through the IEMs occurs prior to ion adsorption inside the micropores, these are crucial in controlling the diffusion. To date, little effort has been made to compare the competitive removal of different cations and anions in CDI to that in MCDI at milliequivalent concentrations.

Another phenomena that is mostly overlooked in this area is the pH fluctuation over one adsorption/desorption cycle. Only recently have He et al. (He et al. 2016) and Gao et al. (Gao et al. 2017) addressed this issue over a range of CDI operating conditions. Tang et al. (Tang et

al. 2017a) probed into details of pH fluctuation in batch mode operation of CDI and MCDI by monitoring the concentration of H_2O_2 and dissolved oxygen, and measuring the electrode potentials. Yet, we believe this phenomenon requires more research especially for a wide range of monovalent and divalent salts.

In this work, we aim to investigate the role of ion affinity to both the carbon electrode and the ion exchange membrane. To cover a wide range of ionic properties, experiments are conducted with NaCl, KCl, $CaCl_2$, $NaNO_3$, and Na_2SO_4 for single and mixed electrolyte solutions in both CDI and MCDI cells. To better understand the competitive electrosoption process, experiments were conducted at milliequivalent concentrations.

Materials and methods

1.1 Materials

In this work, we utilized the analytical grade of all chemicals. Activated carbon (AC Norit SA 4, Cabot Norit Activated Carbon, USA), polyvinylidene fluoride (PVDF, Mw ~530,000, Sigma-Aldrich), N-N dimethylformamide (DMF, 99.8%, Merck Millipore) and graphite sheet (DSN 530, Suzhou Dasen Electronics Material Co., China) were utilized for electrode fabrication. Sodium chloride (NaCl, 99.7%), potassium chloride (KCl, 99%), calcium chloride ($CaCl_2$, 99%), sodium nitrate ($NaNO_3$, 99%) and sodium sulfate (Na_2SO_4, 99%) were used to prepare electrolyte solutions. Solutions were prepared using water purified with a Millipore RIOs Large with a resistance of 1 MΩ cm.

1.2 (M)CDI setup and Electrosorption experiment

Preparation of carbon electrodes using AC Norit SA4 as the carbon source, PVDF as the binder and DMF as the solvent is explained in detail in our previous work (Hassanvand et al. 2017).

Electrodes of 10 cm by 20 cm with a narrow channel of 0.3 cm by 8 cm were fabricated using graphite sheet as the current collector. The carbon content was limited to 6.5 ± 0.5 mg cm^{-2} and the apparent thickness of the electrode materials cast on the current collector was 150 ± 15 μm obtained from SEM images. The prepared electrodes were then characterized using a surface and pore analyzer and cyclic voltammetry. The BET surface area was calculated as 540 ± 4 m^2 g^{-1}, and pore size distribution was indicative of a microporous structure with pore diameters ranging from 0.7 to 1.5 nm. For more details see our previous work (Hassanvand et al. 2017).

The CDI cell consists of two parallel AC electrodes sheets with a 0.9 mm gap which is filled by a non-conductive spacer (Low Foulant spacer 34 mil, Sterlitech). Anion and cation-exchange membranes (Neosepta AMX, thickness of 170 μm, and Neosepta CMX, thickness of 140 μm) are placed in front of the carbon electrodes, to configure the MCDI cell. All layers in the stack are compressed into a poly(carbonate) housing. A DC power module (N6731B, Agilent) in a modular power system mainframe (N6700B, Agilent) was used as the power source and electrical voltage and current across the cell was recorded at a rate of 1 reading per second.

Adsorption was conducted at a constant electrical voltage of 1.5 V while desorption followed at zero voltage in CDI and a reversed polarity of -1.5V in MCDI. In the single-pass mode of operation, the feed solution passed through the cell at a flow rate of 20 ml min^{-1} using a peristaltic pump (NEMA 4X, Watson Marlow) and conductivity and pH (S470-kit, Mettler Toledo) of the effluent was monitored. Conductivity data are converted to salt concentration using the calibration curve corresponding to each salt. Salt adsorption (Q) in ($mmol_{salt}$ g_{carbon}^{-1}) can be calculated as below:

$$Q = \frac{\left(\int_0^{t_{ads}} (C_{in} - C_t).dt\right).\dot{V}}{M_{carbon}} \quad (1)$$

where t_{ads} is the adsorption duration, C_{in} is the inlet salt concentration, C_t is the outlet salt concentration at any time t, $\dot{V}$ is the volumetric flow rate, and M_{carbon} is the total mass of carbon in the electrodes.

Experiments were conducted in a series of single-salt and multi-salt electrolyte solutions using NaCl, KCl, $CaCl_2$, $NaNO_3$, Na_2SO_4. The feed concentration in single-salt and mixed solution experiments was selected as 10 mM for 1:1 salts and 5 mM for $CaCl_2$ and Na_2SO_4 to maintain the ionic strength of the individual ions constant. Each experiment was repeated twice and the results presented are after a number of sufficient absorption/desorption cycles to ensure consistent behavior between each cycle. Table 1 summarized the properties of the selected ions.

Table 1. Physical properties of the studied ions (Mossad and Zou 2012, Nightingale 1959, Robinson and Stokes 1970, Sata 2004).

To further evaluate the cell performance, energy consumption and charge efficiency are determined. Total charge (σ) can be obtained by integrating the electrical current (I_e) passed through the cell over the adsorption time.

$$\sigma = \int_0^{t_{ads}} I_e(t).dt \tag{2}$$

Then knowing the voltage applied (V_{Cell}), energy consumption (Wh m^{-3}) during an adsorption step is calculated from the following equation:

$$E = \frac{V_{Cell} \cdot \sigma}{3600\ (t_{ads}.\dot{V})} \tag{3}$$

Charge efficiency is defined as the ratio of salt removed over the amount of charge transferred through the cell. As efficiency is unitless, the charge is divided by the Faraday constant to be expressed as moles of electrons; and the amount of salt adsorbed is placed in terms of moles into Eq. (4) as below:

$$\Lambda = \frac{Q \,.\, M_{carbon}}{\sigma/_F} \tag{4}$$

The normalized charge efficiency takes account of the requirement for multiple charges to be transferred for a multivalent salt of valence z (Eq. (5))

$$\Lambda_n = \frac{Q_n \,.\, M_{carbon}}{\sigma/_F} = \frac{z.Q.\, M_{carbon}}{\sigma/_F} \tag{5}$$

The concentration of individual cations (Na^+, K^+, Ca^{2+}) was analyzed using Inductively coupled plasma (ICP-OES 720 ES, Varian). The instrument detection limits is 0.03 µg L^{-1} for Ca, 1 µg L^{-1} for Na, and 10 µg L^{-1} for K. An ion-chromatograph (IC-Dionex, ICS-1000) was utilized to determine the concentration of Cl^-, NO_3^- and SO_4^{2-}. A Dionex IONPAC AS-13 column was utilized with a retention time of 15 min and flow rate of 1 mL min^{-1}.

4. Results and discussion

4.1 Comparative Electrosorption capacity of different cations

4.1.1 Feed solutions containing a single salt

To probe the comparative removal of different cations, 10 mM solutions of NaCl, KCl or a 5 mM solution of $CaCl_2$ was fed to the (M)CDI cell in a single pass mode. Fig. 1(a) shows the concentration variation over one cycle in CDI. It was previously reported for CDI that, at the same initial concentration, the hydrated radius governs the sorption capacity (Gabelich et al. 2002). Similarly, in this experiment, KCl is removed marginally faster from the electrolyte in comparison with NaCl in terms of mmol of salt adsorbed per gram of carbon material (Fig. 2(a)). Dykstra et al. (Dykstra et al. 2016b) attributed the marginal selective removal of potassium over sodium in CDI to the higher diffusivity coefficient of the former. Suss (Suss 2017) in his recent publication on EDL modelling achieved greater separation of potassium

189 over sodium by accounting for ion volume exclusion interaction. On the other hand, the
190 difference between monovalent and divalent cations is readily distinguishable. The molar
191 electrosorption capacity of $CaCl_2$ is much lower than that of NaCl and KCl as shown in Fig.
192 2(a), 0.07 mmol g^{-1} for $CaCl_2$ versus 0.13 and 0.15 mmol g^{-1} for NaCl and KCl, respectively.
193 However, it must be noted that for each Ca^{2+} two electrons are consumed. The normalized
194 equivalent capacity (valence × molar adsorption capacity) of $CaCl_2$ is competitive with that of
195 the monovalent ions (0.14 mmol g^{-1}). There are no significant differences in this normalized
196 charge efficiency when equivalent concentrations of the Na^+, K^+ and Ca^{2+} are set equal in the
197 feed.

198 However, it is noticeable that in the CDI cell, the Ca^{2+} adsorbs more slowly than the
199 monovalent ions, with the lowest concentration during adsorption occurring later than for K^+
200 and Na^+; and the concentration at the end of the adsorption cycle not fully recovering.
201 Similarly, while the desorption peak occurs at the same time for all three ions, the recovery to
202 the feed concentration is slightly extended for calcium. These effects probably reflect the
203 slower diffusion rate of calcium, given its larger size.

204 Close inspection of Fig. 1(a) reveals a minor increase at the beginning of each adsorption step,
205 with this increase greatest for KCl. As regeneration occurs at zero voltage, some undesired co-
206 ion adsorption happens during this desorption step. Consequently, when the cell voltage is re-
207 applied during the subsequent adsorption step, an abrupt repulsion of these co-ions occurs,
208 which then results in a repulsion peak (Zhao et al. 2013). The extent of co-ion adsorption is
209 greatest for KCl consistent with the normalized capacity and its small hydrated radius.

210 In the next series of experiments, ion-exchange membranes were placed in front of the
211 electrodes to provide an MCDI arrangement (Fig. 1(b)). In these experiments, while the
212 adsorption duration was kept similar to CDI, a shorter desorption time was required as

described in Section 3.2 above. When using IEMs, there are fewer differences in concentrations between ions and the charge efficiency is significantly higher (Fig. 2(b)) as has been noted by other authors (Zhao et al. 2012a, Zhao et al. 2013). The repulsion peak at the beginning of the adsorption step is also no longer present, confirming that the peak observed in CDI arises from co-ion repulsion and does not arise from immobile chemical charges or inverted CDI, as described by Biesheuvel et al. (Biesheuvel et al. 2015) and Gao et al. (Gao et al. 2016).

Fig. 1. Changes in effluent salt concentration obtained experimentally in (a) CDI, and (b) MCDI cell in the treatment of NaCl, KCl and $CaCl_2$ individually as single salt experiments.

Fig. 2. Experimental salt adsorption and charge efficiency of (a) CDI, and (b) MCDI cell in the treatment of NaCl, KCl and $CaCl_2$ individually as single salt experiments.

In the MCDI cell the salt adsorption of NaCl is slightly higher than that of KCl, although they both have similar charge efficiency, 94.8 % and 96.2 %, respectively (Fig. 2(b)). It is apparent that, for these monovalent ions, the effect of hydrated radii is no longer relevant, suggesting that the IEMs themselves are now governing the mass transfer. Similarly, with equivalent ionic strength of cations, $CaCl_2$ is behaving very similar to the monovalent electrolytes in contrast to what was observed in CDI. While the salt adsorption capacity is identical, there is evidence of marginally smaller charge efficiency, which may arise from the slow diffusion of Ca^{2+} through the IEM and into the porous carbon electrode.

Molar salt adsorption was determined to be 0.12 mmol g^{-1} for $CaCl_2$ flowing in the MCDI cell which has almost doubled in comparison to the CDI case. Indeed, the normalized charge efficiency of MCDI is uniformly high. This enhancement is owing to co-ion blockage and regeneration at reversed voltage when using MCDI. When the polarity is reversed, the counter-ions, i.e. the ions having opposite charge to the electrode during adsorption, not only leave the micropores of the carbon electrodes, but the macropores also become depleted. Hence, in the

following adsorption step, there is more driving force for the ions of opposite charge to diffuse through the macropores and adsorb into the electrical double-layers inside the micropores. Conversely, in CDI, when the voltage drops to zero, the adsorbed ions are repulsed; however, their concentration in the macropores of the carbon only drops to that of the bulk stream.

4.1.2 Feed solutions containing a salt mixture

Deionization experiments were next conducted using a single solution containing a mixture of 10 mM of NaCl, KCl and 5 mM $CaCl_2$ in a single-pass mode. As a salt mixture is used, the concentrations of each salt must be determined by ion analysis, rather than simple conductivity. Hence, after observing five consecutive stable adsorption-desorption cycles as evidenced by conductivity monitoring, samples were taken at the exit of the cell for individual ion analysis at a number of time points during the ensuing cycle. Fig. 3 depicts the result of competitive removal of the three different cations in CDI and MCDI, respectively, while Table 2 provides the equivalent adsorption capacity, based on an integration of the areas over the respective absorption and desorption periods.

As shown in Fig. 3(a), for CDI, in the early stages of electrosorption, the potassium and sodium ions recover from co-ion repulsion faster and adsorb onto the cathode faster than calcium. However, after five minutes of adsorption, the effluent concentration of monovalent ions is higher than that of calcium, which now dominates the adsorption process. Similarly, potassium is the first to desorb from the cathode. These observations are similar to that reported previously in CDI (Seo et al. 2010, Zhao et al. 2012b).

Fig. 3. Competitive electrosorption of Na^+, K^+ and Ca^{2+} based on ion analysis of the effluent stream in (a) CDI, (b) MCDI in the mixed salt experiment. Symbols represent ion analyses, while lines are a guide for the eye.

253 **Table 2.** Equivalent adsorption of each ion oven one cycle of CDI and MCDI in the case of mixed
254 cations obtained from Fig. 3.

255 The preferential ion sorption can be explained through the interplay of two phenomena: (i)
256 diffusion kinetics, (ii) adsorption equilibria. Due to the smaller hydrated radii of monovalent
257 ions, they diffuse more rapidly into the micropores, resulting in initially greater uptake of KCl
258 > NaCl > $CaCl_2$. However, adsorption equilibria, either determined experimentally (Hou and
259 Huang 2013) or predicted by modified-Donnan EDL-theory (Zhao et al. 2012b), indicates that
260 Ca^{2+} is more strongly adsorbed and will ultimately replace these ions in a mixed ion solution.
261 Zhao et al. (Zhao et al. 2012b) demonstrated these effects to show how the operating process
262 can be manipulated to achieve an effluent rich in either monovalent ions (over short time
263 frames) or divalent ions (over long timeframes). Seo at al. (Seo et al. 2010) also showed that
264 sodium removal efficiency is lower than calcium and magnesium owing to substitution of the
265 adsorbed Na^+ by divalent ions over time. Hou and Huang (Hou and Huang 2013) find that in
266 an equimolar mixture of salts, Ca^{2+} is adsorbed most strongly, followed by K^+ and then Na^+.
267 The activated carbon used by Hou and Huang showed a wider pore size distribution to that
268 used in this work (Hassanvand et al. 2017), which might facilitate the diffusion of larger
269 hydrated ions such as calcium. Our own results show K^+ with the strongest normalized sorption
270 capacity, but this is closely followed by Ca^{2+} (Table 2).Ion analysis shows a different trend for
271 the MCDI experiments. As noted in the single salt experiments, it is apparent that there is much
272 less significant discrepancy among the effluent concentration of each cation during the
273 adsorption step when using IEMs (Fig. 3(b)). Similar to CDI, Ca^{2+} adsorption dominates after
274 an initial period where K^+ is more dominant. However, the differences in ion concentration is
275 more noticeable during the desorption step. It is clear that Ca^{2+} leaves the MCDI cell faster
276 relative to monovalent ions. This rapid release is somewhat unexpected given the large size
277 and hence slow diffusion rate of the Ca^{2+} ion. We believe that this effect arises from the large

capacity for Ca^{2+} uptake within the cation exchange membrane itself. It is well known that due to the strong electrostatic force between divalent cations and the fixed charged groups within an IEM, that divalent counterions will be dominant within this phase in mixed cation systems. This is the basis of Donnan exclusion theory (Mulder 1996, Strathmann 2004) and has been observed by a number of workers including (Joshi and Kwak 1981) Ayala-Bribiesca et al. (Ayala-Bribiesca et al. 2006) and Shee et al. (Shee et al. 2008). As a result, when the polarity is reversed, divalents are expelled quickly. In contrast, monovalents require more time to appear at the cell exit as they need to leave the micro and macro pores of the carbon, and then diffuse through the IEMs. Potassium's higher adsorption and desorption rate in comparison to sodium can be attributed to its smaller hydrated radii and higher diffusivity coefficient which helps it to electromigrate faster in comparison to Na^{+}.

4.2 Comparative Electrosorption capacity of different anions

4.2.1 Feed solutions containing a single salt

Fig. 4(a) shows how the effluent concentration varies over one cycle out of five consecutive stable cycles when running single-salt experiments in CDI where the anion was varied. The total salt adsorption of NaCl and $NaNO_3$ are identical within experimental error (Fig. 7(a)), although other workers have found that NO_3^- has greater sorption capacity than Cl^- (Li et al. 2016). The differences in the shape of the sorption and desorption curves between these two salts probably reflect the much greater co-ion adsorption observed for NO_3^-, as indicated by the large peak at the beginning of the desorption cycle, when these adsorbed ions are repulsed by the application of a charge. It is known that NO_3^- is a relatively hydrophobic anion, as indicated by a low ratio of hydrated to ionic radius (Hydration ratio, Table 1) (Li et al. 2016), and this results in significant adsorption to the carbon when there is no charge applied. This substantial co-ion adsorption and desorption results in low charge efficiency (Fig. 7(a)) and is also the reason that the net sorption capacity is not greater than that for NaCl. The normalized salt

adsorption for Na_2SO_4 is low, relative to both NaCl and $NaNO_3$ which may relate to slow diffusion of the SO_4 anion due to its larger hydrated radius – this is reflected in a slightly later adsorption minimum concentration and desorption maximum concentration. The charge efficiency is comparable to $NaNO_3$, although there is no evidence of co-ion repulsion effects in this case. This again may be because the slow diffusion rate results in a broader and flatter co-ion repulsion peak that is not evident in the experimental data.

As with the cation experiments, the performance becomes more uniform when IEMs are installed for the MCDI experiments (Fig. 4(b)) with significantly higher adsorption capacity and charge efficiency in comparison to that of CDI. The peaks at the beginning of the adsorption cycle are also again absent. This is because co-ion adsorption now cannot occur and all charge is consumed in adsorbing the anions onto the anode. The normalized charge efficiency for NaCl and $NaNO_3$ is identical and close to one which is representative of an energy efficient technique. Similar to the data for $CaCl_2$ in Fig. 2(b), the charge efficiency for Na_2SO_4 is slightly lower, which can be attributed to a smaller diffusivity coefficient of the divalent ions through the IEMs and into the carbon.

Fig. 4. Changes in effluent salt concentration in (a) CDI, and (b) MCDI cell in the treatment of NaCl, $NaNO_3$ and Na_2SO_4 individually as single salt experiments.

Fig. 5. Experimental salt adsorption and charge efficiency of (a) CDI, and (b) MCDI cell in the treatment of NaCl, $NaNO_3$ and Na_2SO_4 individually as single salt experiments.

4.2.2 Feed solutions containing a salt mixture

Ion analysis results of the effluent stream in a mixed salt solution of NaCl, $NaNO_3$ and Na_2SO_4 are shown in Fig. 6 from which the equivalent adsorption has been obtained and presented in Table 3. During the adsorption step in mixed salt CDI, SO_4^{2-} and Cl^- are adsorbed at a faster rate in the early electrosorption period. Similar to the behavior of the multi cation experiment,

the concentration of the first two adsorbed ions then recovers quickly to be replaced by the NO_3^- ion. As discussed above, the strong hydrophobicity of NO_3^- means that a significant concentration is adsorbed onto the cathode during the preceding desorption step and so the initial 2-3 minutes of the adsorption cycle is dominated by repulsion of these co-ions. Once these ions have been recovered, the stronger sorption capacity of NO_3^- allows it to replace the Cl^- and SO_4^{2-} ions. Chen et al. (Chen et al. 2015) investigated the competitive electrosorption of mixed Cl^- and NO_3^- and mixed Cl^- and SO_4^{2-} solutions and reported a similar ion substitution phenomenon for NO_3^-. They compared this behavior to ion exchange processes in which NO_3^- is similarly selectively adsorbed relative to Cl^-. In another work, Tang et al. (Tang et al. 2015) attributed the higher ion removal rate of nitrate to a stronger non-electrostatic attraction between carbon and this ion.

As shown in Fig. 6(b), similar behavior to that of cation mixed salt desalination (Fig. 3(b)) was observed for MCDI. Cl^-, NO_3^- and SO_4^{2-} were removed from the salty stream at similar rates during adsorption, as a result, the salt adsorptions of all anions are quite similar. Operating MCDI under constant current, Tang et al. (Tang et al. 2017b) reported that the sorption ratio of sulfate to chloride is a function of electrical current applied. Therefore the trend we observed here might be slightly different at lower or higher cell voltages. Nonetheless, the fact that equimolar concentrations of sulfate and chloride was used by these authors (instead of milliequivalent concentrations) might explain the higher adsorption of sulfate in their study in comparison to ours.

The effect of ion properties is more noticeable when it comes to desorbing the ions from carbon electrode. There is a sharper peak of sulfate desorption in the first two minutes of desorption. As discussed for calcium above, we believe that this is due to the greater sorption of this divalent anion within the anion exchange membrane in a mixed ion solution. The hydrated radii

of Cl^- and NO_3^- are similar (see Table 1) and therefore, they are desorbed at comparable rates. However, as shown in Table 3, the equivalent adsorption capacity for NO_3^- is highest, reflecting its greater affinity for the carbon electrodes (lower hydration ratio).

From Fig. 3(b) and Fig. 6(b), it is apparent that diffusion through the membrane matrix can be the rate controlling step which synchronizes the transport of the different cations and anions. Most importantly, the membranes act as a storage reservoir for divalent ions, which means that desorption of these ions is more rapid. This reinforces the hypothesis that during desorption, ionic charge is the governing factor in MCDI, followed by hydrated radii. The more the ionic charge and the smaller the hydrated radii, the faster an individual ion is desorbed. This is an important finding from an application point of view as it shows that the use of ion exchange membranes can significantly alter the selective electrosorption mechanisms of CDI. Careful control of the desorption cycle time could provide a solution concentrated in calcium sulfate. This salt is a well-known fouling agent and hence its removal could facilitate a downstream reverse osmosis or evaporation operation.

As discussed in different sections of this study, comparing CDI experimental performance of two different works seems quite complicated as there any many critical variables involved, including the carbon properties (specific surface area, pore size distribution, surface groups, and specific capacitance), cell configuration (electrode thickness, distance between the electrodes, and spacer type), and operational parameters (feed concentration, flow rate, and applied voltage). This issue further highlights the importance of developing a comprehensive dynamic transport model in this area which can reflect the effect of such properties. Verification of desalination rate of different salts in CDI and MCDI in a single-pass mode enables us to predict the performance of these energy efficient techniques in a wide range of operational condition and in treating multi-component feed.

Fig. 6. Competitive electrosorption of Cl^-, NO_3^- and SO_4^{2-} by ion analysis of the effluent stream in (a) CDI, (b) MCDI in the mixed salt experiment. Symbols represent ion analyses, while lines are a guide for the eye.

375 **Table 3.** Equivalent adsorption of each ion oven one cycle of CDI and MCDI in the case of mixed
376 anions obtained from Fig. 6.

377 To test the stack capacity after the completion of all experiments, NaCl removal was compared
378 with the initial performance. As the effluent salt concentration was identical to this initial
379 performance, it can be claimed that the capacity of (M)CDI cell remained constant and thus
380 that (M)CDI is a stable desalination method.

381 ### 4.3 pH fluctuation

382 The pH fluctuation that occurs during adsorption and desorption of various salts during CDI
383 and MCDI has not been studied comprehensively. We believe that monitoring the pH change
384 over one cycle of adsorption and desorption is helpful to probe this issue in more detail. It
385 should be noted that the data presented here is for a pair of carbon electrodes that had been
386 used for at least 20 cycles. The pH of solutions that have been exposed to a fresh electrode
387 fluctuates more significantly, as the surface of the fresh carbon contains functional groups that
388 are initially reactive with water.

389 Fig. 7(a,b) demonstrate the fluctuation of effluent pH in CDI and MCDI for single-salt
390 electrolytes passing through the cell in a single pass mode. While all the desalination
391 experiments start with a feed solution of pH of 6.2 ± 0.3, the initial effluent pH is influenced
392 by the previous treatment cycles. During adsorption of salt solution in the CDI configuration,
393 the pH first increases and then decreases (Fig. 7(a)). The pH fluctuation reveals that Faradaic
394 reactions (oxidation-reduction) occurs in tandem with ion electrosorption (non-faradaic effect)

(He et al. 2016). This dramatic fluctuation in pH could lead to salt precipitation and subsequent fouling of the electrodes in industrial applications, which is undesirable. Lee et al. (Lee et al. 2010) observed a similar pH trend at cell voltages above 1.0 V. They attributed two phenomena to this pH change: (i) reduction of dissolved oxygen at the cathode, see Eq. (6); and (ii) Oxidation of anions such as Cl^- at the anode which is then followed by disproportionation of Cl_2 (Lee et al. 2010, Zhao et al. 2014). The oxygen reduction reaction may occur through a four-electron (Eq. (6)) or two-electron (Eq. (7)) pathway where the latter is followed by reduction of peroxide as shown in Eq. (8) (Kinoshita 1988, Song and Zhang 2008).

$$O_2 + 2H_2O + 4\,e^- \rightarrow 4OH^- \qquad E^0 = 0.401\,V \tag{6}$$

$$O_2 + H_2O + 2\,e^- \rightarrow HO_2^- + OH^- \qquad E^0 = -0.065\,V \tag{7}$$

$$HO_2^- + H_2O + 2\,e^- \rightarrow 3OH^- \qquad E^0 = 0.867\,V \tag{8}$$

$$2Cl^- \rightarrow Cl_2(aq) + 2\,e^- \qquad E^0 = 1.360\,V \tag{9}$$

$$Cl_2(aq) + H_2O \rightarrow HCl + HOCl \tag{10}$$

Therefore oxygen reduction in the early stages of the adsorption cycle results in a pH increase through hydroxyl ion production. At ambient pressure and temperature, the maximum oxygen solubility in a solution of 10 mM salt is 8.2 ± 0.1 mg L^{-1} which can result in a pH of around 11 corresponding to Eq. (6) or a combination of Eqs. (7) and (8). For a closed system, as might be used in an industrial application, this value is expected to be lower. It is worth noting that while Tang et al. (Tang et al. 2017a) monitored oxygen reduction reactions in acidic solutions by H_2O_2 formation, oxygen reduction will proceed via Eq. (6) or (7) in neutral or alkaline solutions(Song and Zhang 2008).

However, it is apparent that Cl^- oxidation (Eqs. 9 and 10) is not a valid justification for the subsequent drop in pH, as this sharp drop can also be observed for other anions, $NaNO_3$ and

Na_2SO_4. He et al. (He et al. 2016) measured HOCl concentration and also argued that Cl^- oxidation was not the cause. That research group suggested that, at 1.5 V, water splitting (Eq. (11)) and carbon oxidation (Eq. (12)) most likely contribute to the pH decrease after reaching an early peak. They argued that the redox potential would be lower at high pH values which makes these reactions feasible (He et al. 2016).

$$\frac{1}{2}H_2O \rightarrow \frac{1}{4}O_2 + H^+ + e^- \qquad E^0 = 1.23\,V \tag{11}$$

$$\frac{1}{4}C + \frac{1}{2}H_2O \rightarrow \frac{1}{4}CO_2 + H^+ + e^- \qquad E^0 = 0.7 - 0.9\,V \tag{12}$$

Nonetheless, as Eq. (12) occurs, carbon is consumed which leads to electrode mass loss (Porada et al. 2013). Considering the stability of the (M)CDI device noted above, the likelihood of significant carbon oxidation is quite low. If carbon material at the anode was significantly involved in electrochemical reactions, the desalination performance would diminish with time.

Fig. 7. Effluent pH values in (a) CDI, and (b) MCDI during one adsorption desorption cycle of single salts experiments.

It is noteworthy that while the pH change during salt adsorption in CDI appears large, with a peak of 10.5 and a minimum of 3.5, the change in H^+ concentration is limited to only 0.3 mM. This is negligible in comparison with the changes in salt concentration reported in this work. As a result, the changes in the H^+ concentration do not affect the salt concentration measurements significantly. It is also worth mentioning that the large pH swing is also related to the relatively high voltage (1.5 V) used in these experiments. In processes sensitive to such pH fluctuations, we suggest operating at lower voltage despite the fact the salt removal would decrease.

On the other hand, as represented in Fig. 7(b), the range of pH change in MCDI is smaller than that of CDI, especially the initial increase. There are some possible explanations for this.

Firstly, placing the CEM in front of the cathode reduces the access of dissolved oxygen to the carbon surface. This argument was also used in the recent publication by Tang et al. (Tang et al. 2017a). Secondly, for the oxygen that does reach the cathode, the OH^- produced (see oxygen reduction reactions) cannot easily penetrate through the cation exchange membrane to reach the bulk solution. As the initial pH jump does not occur; therefore, the redox potentials of reactions (11) and (12) are not met. Finally, not only is the occurrence of these last two equations reduced, but the transport of the H^+ ions produced into the bulk stream is hindered by the anion-exchange membrane. We also assume that any hydroxyl and hydronium ions so trapped behind each ion-exchange membrane can enhance the counter-ion attraction. Marginally different pH patterns for Na_2SO_4 and $CaCl_2$ might reflect greater water splitting, as reflected in the slightly lower charge efficiency noted for these systems, but this would require further investigation.

A better understanding of the pH fluctuation would assist in the development of mathematical models to account for the contribution of hydronium and hydroxyl ions. Recently, Dykstra et al. (Dykstra et al. 2017) incorporated one pathway for oxygen reduction and carbon oxidation into an ion transport model of MCDI to calculate the pH changes. However, given the much greater pH fluctuation in the case of CDI, all Faradaic reactions must be added to the relevant ion transport models to calculate the portion of voltage being dissipated within these side reactions.

Conclusion

In this work, activated carbon electrodes were prepared and then were utilized in a CDI and (M)CDI setup. Single salt electrolyte solutions of NaCl, KCl, $CaCl_2$, $NaNO_3$, Na_2SO_4 were tested as were solutions containing mixtures of three cations and three anions. The results show that the charge efficiency of NO_3^- and SO_4^{2-} is lower in CDI than for other anions which can

be attributed to strong co-ion adsorption and to slow rates of diffusion. Salt adsorption and charge efficiency boosted significantly when IEMs were introduced in front of the electrodes. Importantly, once IEMs were in place, there was a change in the order of desorption, with divalent cations and anions giving a stronger desorption peak. We believe that this relates to the IEMs acting as storage reservoirs for these ions reducing the path length of diffusion before release. The limited pH change in MCDI adds to the advantage of this technique over CDI since a vigorous pH increase and decrease is not favorable to fresh water production.

Acknowledgements

Armineh Hassanvand acknowledges The University of Melbourne for the IPRS (International Postgraduate Research Scholarship) and APA (Australian Postgraduate Awards) scholarships, which are funded by the Australian Government. George Chen and Sandra Kentish acknowledge research funding from the Australian Research Council Industrial Transformation Research Program (ITRP) scheme (Project Number IH120100005). The ARC Dairy Innovation Hub is a collaboration between The University of Melbourne, The University of Queensland and Dairy Innovation Australia Ltd. George Chen acknowledges support from an Early Career Researcher (ECR) Grant awarded by the Melbourne School of Engineering, The University of Melbourne. We are grateful to Professor Benny Freeman (The University of Texas at Austin) who provided expertise in ion transport through IEMs. We would also like to acknowledge the Particulate Fluid Processing Centre at the University of Melbourne) for infrastructure support.

References

Asquith, B.M., Meier-Haack, J. and Ladewig, B.P. (2015) Poly(arylene ether sulfone) copolymers as binders for capacitive deionization activated carbon electrodes. Chem. Eng. Res. Des. 104, 81-91.

Ayala-Bribiesca, E., Araya-Farias, M., Pourcelly, G. and Bazinet, L. (2006) Effect of concentrate solution pH and mineral composition of a whey protein diluate solution on membrane fouling formation during conventional electrodialysis. Journal of Membrane Science 280(1), 790-801.

Biesheuvel, P.M., Hamelers, H.V.M. and Suss, M.E. (2015) Theory of Water Desalination by Porous Electrodes with Immobile Chemical Charge. Colloids Interface Sci. Commun. 9, 1-5.

Biesheuvel, P.M. and van der Wal, A. (2010) Membrane capacitive deionization. J. Membr. Sci. 346(2), 256-262.

Biesheuvel, P.M., Zhao, R., Porada, S. and van der Wal, A. (2011) Theory of membrane capacitive deionization including the effect of the electrode pore space. Journal of Colloid and Interface Science 360(1), 239-248.

Bouhadana, Y., Avraham, E., Soffer, A. and Aurbach, D. (2010) Several basic and practical aspects related to electrochemical deionization of water. AIChE J. 56(3), 779-789.

Chen, Z., Zhang, H., Wu, C., Wang, Y. and Li, W. (2015) A study of electrosorption selectivity of anions by activated carbon electrodes in capacitive deionization. Desalination 369, 46-50.

Dykstra, J., Zhao, R., Biesheuvel, P. and Van der Wal, A. (2016a) Resistance identification and rational process design in Capacitive Deionization. Water Research 88, 358-370.

498 Dykstra, J.E., Dijkstra, J., van der Wal, A., Hamelers, H.V.M. and Porada, S. (2016b) On-line
499 method to study dynamics of ion adsorption from mixtures of salts in capacitive deionization.
500 Desalination 390, 47-52.

501 Dykstra, J.E., Keesman, K.J., Biesheuvel, P.M. and van der Wal, A. (2017) Theory of pH
502 changes in water desalination by capacitive deionization. Water Research 119, 178-186.

503 Gabelich, C.J., Tran, T.D. and Mel Suffet, I.H. (2002) Electrosorption of Inorganic Salts from
504 Aqueous Solution Using Carbon Aerogels. Environ. Sci. Technol. 36(13), 3010-3019.

505 Gao, X., Omosebi, A., Holubowitch, N., Landon, J. and Liu, K. (2017) Capacitive Deionization
506 Using Alternating Polarization: Effect of Surface Charge on Salt Removal. Electrochimica
507 Acta 233, 249-255.

508 Gao, X., Porada, S., Omosebi, A., Liu, K.L., Biesheuvel, P.M. and Landon, J. (2016)
509 Complementary surface charge for enhanced capacitive deionization. Water Res. 92, 275-282.

510 Han, L., Karthikeyan, K.G., Anderson, M.A. and Gregory, K.B. (2014) Exploring the impact
511 of pore size distribution on the performance of carbon electrodes for capacitive deionization.
512 Journal of Colloid and Interface Science 430(0), 93-99.

513 Hassanvand, A., Chen, G.Q., Webley, P.A. and Kentish, S.E. (2017) Improvement of MCDI
514 operation and design through experiment and modelling: Regeneration with brine and optimum
515 residence time. Desalination 417, 36-51.

516 He, D., Wong, C.E., Tang, W., Kovalsky, P. and Waite, T.D. (2016) Faradaic Reactions in
517 Water Desalination by Batch-Mode Capacitive Deionization. Environmental Science &
518 Technology Letters.

519 Hou, C.-H. and Huang, C.-Y. (2013) A comparative study of electrosorption selectivity of ions
520 by activated carbon electrodes in capacitive deionization. Desalination 314(0), 124-129.

521 Huyskens, C., Helsen, J. and de Haan, A.B. (2013) Capacitive deionization for water treatment:
522 Screening of key performance parameters and comparison of performance for different ions.
523 Desalination 328(0), 8-16.

524 Joshi, Y.M. and Kwak, J.C.T. (1981) The binding of divalent metal ions to polyelectrolytes in
525 mixed counterion systems. Biophysical Chemistry 13(1), 65-75.

526 Kim, J.S., Jeon, Y.S. and Rhim, J.W. (2016) Application of poly(vinyl alcohol) and polysulfone
527 based ionic exchange polymers to membrane capacitive deionization for the removal of mono-
528 and divalent salts. Separation and Purification Technology 157, 45-52.

529 Kim, Y.-J. and Choi, J.-H. (2012) Selective removal of nitrate ion using a novel composite
530 carbon electrode in capacitive deionization. Water Research 46(18), 6033-6039.

531 Kim, Y.-J., Hur, J., Bae, W. and Choi, J.-H. (2010) Desalination of brackish water containing
532 oil compound by capacitive deionization process. Desalination 253(1–3), 119-123.

533 Kim, Y.-J., Kim, J.-H. and Choi, J.-H. (2013) Selective removal of nitrate ions by controlling
534 the applied current in membrane capacitive deionization (MCDI). Journal of Membrane
535 Science 429, 52-57.

536 Kinoshita, K. (1988) Carbon: electrochemical and physicochemical properties.

537 Lee, J.-H., Bae, W.-S. and Choi, J.-H. (2010) Electrode reactions and adsorption/desorption
538 performance related to the applied potential in a capacitive deionization process. Desalination
539 258(1), 159-163.

540 Li, Y., Zhang, C., Jiang, Y., Wang, T.-J. and Wang, H. (2016) Effects of the hydration ratio on
541 the electrosorption selectivity of ions during capacitive deionization. Desalination 399, 171-
542 177.

543 Liu, Y., Nie, C., Liu, X., Xu, X., Sun, Z. and Pan, L. (2015) Review on carbon-based composite
544 materials for capacitive deionization. RSC Adv. 5(20), 15205-15225.

545 Mossad, M., Zhang, W. and Zou, L. (2013) Using capacitive deionization for inland brackish
546 groundwater desalination in a remote location. Desalination 308, 154-160.

547 Mossad, M. and Zou, L. (2012) A study of the capacitive deionisation performance under
548 various operational conditions. Journal of hazardous materials 213–214(0), 491-497.

549 Mulder, M. (1996) Basic Principles of Membrane Technology, Dordrecht; Boston: Kluwer
550 Academic.

551 Nightingale, E.R., Jr. (1959) Phenomenological theory of ion solvation. Effective radii of
552 hydrated ions. J. Phys. Chem. 63, 1381-1387.

553 Porada, S., Zhao, R., van der Wal, A., Presser, V. and Biesheuvel, P.M. (2013) Review on the
554 science and technology of water desalination by capacitive deionization. Progress in Materials
555 Science 58(8), 1388-1442.

556 Robinson, R.A. and Stokes, R.H. (1970) Electrolyte solutions, [electronic resource] the
557 measurement and interpretation of conductance, chemical potential, and diffusion in solutions
558 of simple electrolytes, London, Butterworths [1965, reprinted 1970]2d ed., rev.

559 Sata, T. (2004) Ion exchange membranes: preparation, characterization, modification and
560 application, Royal Society of Chemistry.

561 Seo, S.-J., Jeon, H., Lee, J.K., Kim, G.-Y., Park, D., Nojima, H., Lee, J. and Moon, S.-H. (2010)
562 Investigation on removal of hardness ions by capacitive deionization (CDI) for water softening
563 applications. Water Research 44(7), 2267-2275.

564 Shee, F.L.T., Angers, P. and Bazinet, L. (2008) Microscopic approach for the identification of
565 cationic membrane fouling during cheddar cheese whey electroacidification. Journal of Colloid
566 and Interface Science 322(2), 551-557.

567 Song, C. and Zhang, J. (2008) Electrocatalytic oxygen reduction reaction. PEM Fuel Cell
568 Electrocatalysts and Catalyst Layers: Fundamentals and Applications 1, 92.

569 Strathmann, H. (2004), Ion-exchange membrane separation processes, Amsterdam; Boston:
570 Elsevier.

571 Subramani, A. and Jacangelo, J.G. (2015) Emerging desalination technologies for water
572 treatment: A critical review. Water Res. 75, 164-187.

573 Suss, M.E. (2017) Size-based ion selectivity of micropore electric double layers in capacitive
574 deionization electrodes. arXiv preprint arXiv:1704.04156.

575 Tang, W., He, D., Zhang, C., Kovalsky, P. and Waite, T.D. (2017a) Comparison of Faradaic
576 reactions in capacitive deionization (CDI) and membrane capacitive deionization (MCDI)
577 water treatment processes. Water Research 120, 229-237.

578 Tang, W., He, D., Zhang, C. and Waite, T.D. (2017b) Optimization of sulfate removal from
579 brackish water by membrane capacitive deionization (MCDI). Water Research 121, 302-310.

580 Tang, W., Kovalsky, P., He, D. and Waite, T.D. (2015) Fluoride and nitrate removal from
581 brackish groundwaters by batch-mode capacitive deionization. Water Res. 84, 342-349.

582 Wang, C., Song, H., Zhang, Q., Wang, B. and Li, A. (2015) Parameter optimization based on
583 capacitive deionization for highly efficient desalination of domestic wastewater biotreated
584 effluent and the fouled electrode regeneration. Desalination 365, 407-415.

585 Xu, P., Drewes, J.E., Heil, D. and Wang, G. (2008) Treatment of brackish produced water using
586 carbon aerogel-based capacitive deionization technology. Water Research 42(10–11), 2605-
587 2617.

588 Zhao, R., Biesheuvel, P.M. and van der Wal, A. (2012a) Energy consumption and constant
589 current operation in membrane capacitive deionization. Energy Environ. Sci. 5(11), 9520-
590 9527.

591 Zhao, R., van Soestbergen, M., Rijnaarts, H.H.M., van der Wal, A., Bazant, M.Z. and
592 Biesheuvel, P.M. (2012b) Time-dependent ion selectivity in capacitive charging of porous
593 electrodes. J. Colloid Interface Sci. 384(1), 38-44.

594 Zhao, Y., Hu, X.-m., Jiang, B.-h. and Li, L. (2014) Optimization of the operational parameters
595 for desalination with response surface methodology during a capacitive deionization process.
596 Desalination 336, 64-71.

597 Zhao, Y., Wang, Y., Wang, R., Wu, Y., Xu, S. and Wang, J. (2013) Performance comparison
598 and energy consumption analysis of capacitive deionization and membrane capacitive
599 deionization processes. Desalination 324, 127-133.

600

601

Figure Captions:

Fig. 1. Changes in effluent salt concentration obtained experimentally in (a) CDI, and (b) MCDI cell in the treatment of NaCl, KCl and $CaCl_2$ individually as single salt experiments.

Fig.2. Experimental salt adsorption and charge efficiency of (a) CDI, and (b) MCDI cell in the treatment of NaCl, KCl and $CaCl_2$ individually as single salt experiments.

Fig.3. Competitive electrosorption of Na^+, K^+ and Ca^{2+} based on ion analysis of the effluent stream in (a) CDI, (b) MCDI in the mixed salt experiment. Symbols represent ion analyses, while lines are a guide for the eye.

Fig. 4. Changes in effluent salt concentration in (a) CDI, and (b) MCDI cell in the treatment of NaCl, $NaNO_3$ and Na_2SO_4 individually as single salt experiments.

Fig. 5. Experimental salt adsorption and charge efficiency of (a) CDI, and (b) MCDI cell in the treatment of NaCl, $NaNO_3$ and Na_2SO_4 individually as single salt experiments.

Fig.6. Competitive electrosorption of Cl^-, NO_3^- and SO_4^{2-} by ion analysis of the effluent stream in (a) CDI, (b) MCDI in the mixed salt experiment. Symbols represent ion analyses, while lines are a guide for the eye.

Fig. 7. Effluent pH values in (a) CDI, and (b) MCDI during one adsorption desorption cycle of single salts experiments.

620 **Table Captions:**

621 **Table 1.** Physical properties of the studied ions (Mossad and Zou 2012, Nightingale 1959,
622 Robinson and Stokes 1970, Sata 2004).

623 **Table 2.** Equivalent adsorption of each ion oven one cycle of CDI and MCDI in the case of
624 mixed cations obtained from Fig. 3.

625 **Table 3.** Equivalent adsorption of each ion oven one cycle of CDI and MCDI in the case of
626 mixed anions obtained from Fig. 6.

627

628

629

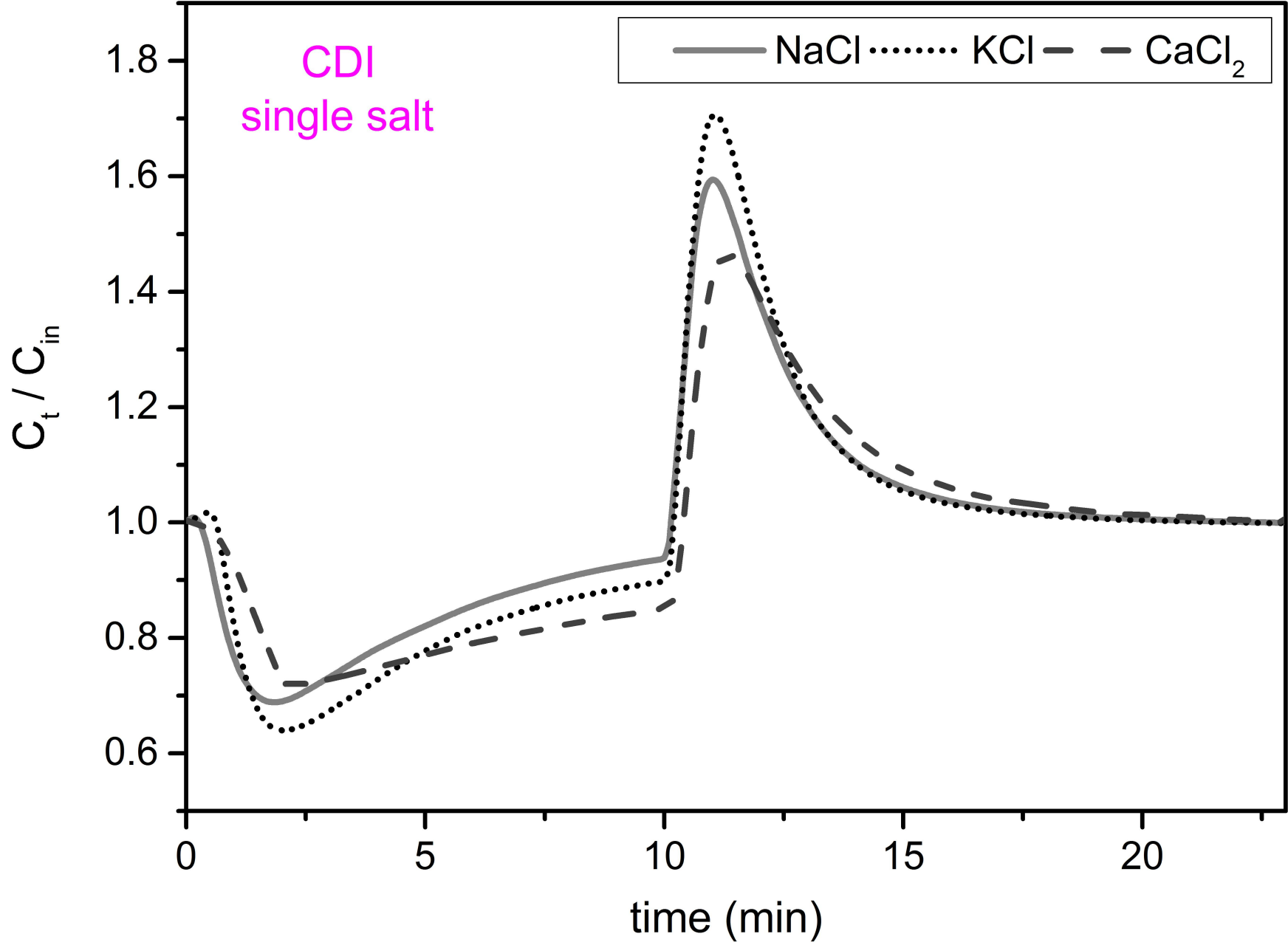
CDI
single salt
NaCl
KCl
CaCl2
1.8
1.6
1.4
1.2
1.0
0.8
0.6
Ct / Cin
0
5
10
15
20
time (min)

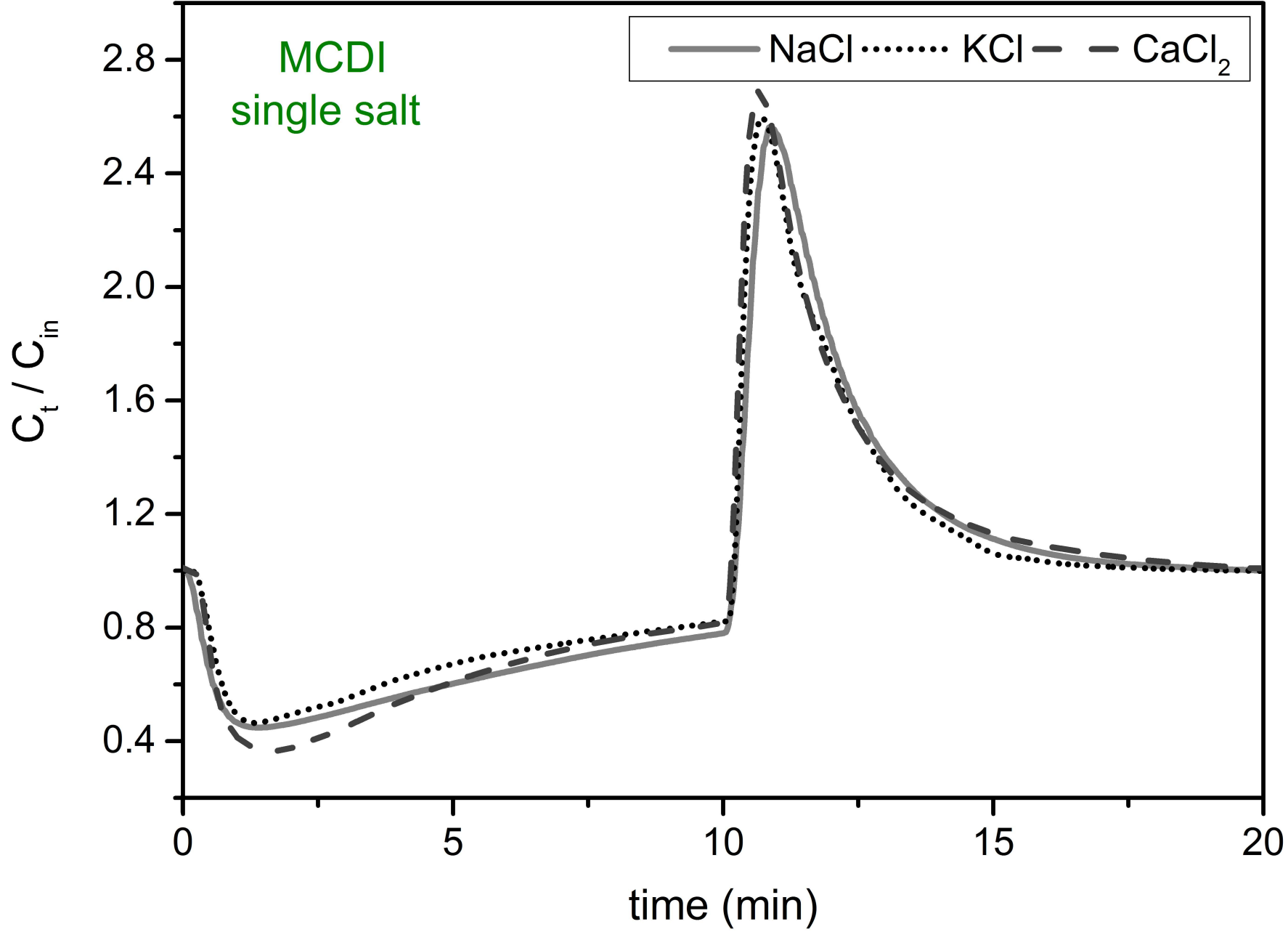
MCDI
single salt
NaCl
KCl
CaCl2
2.8
2.4
2.0
1.6
1.2
0.8
0.4
Ct / Cin
0
5
10
15
20
time (min)

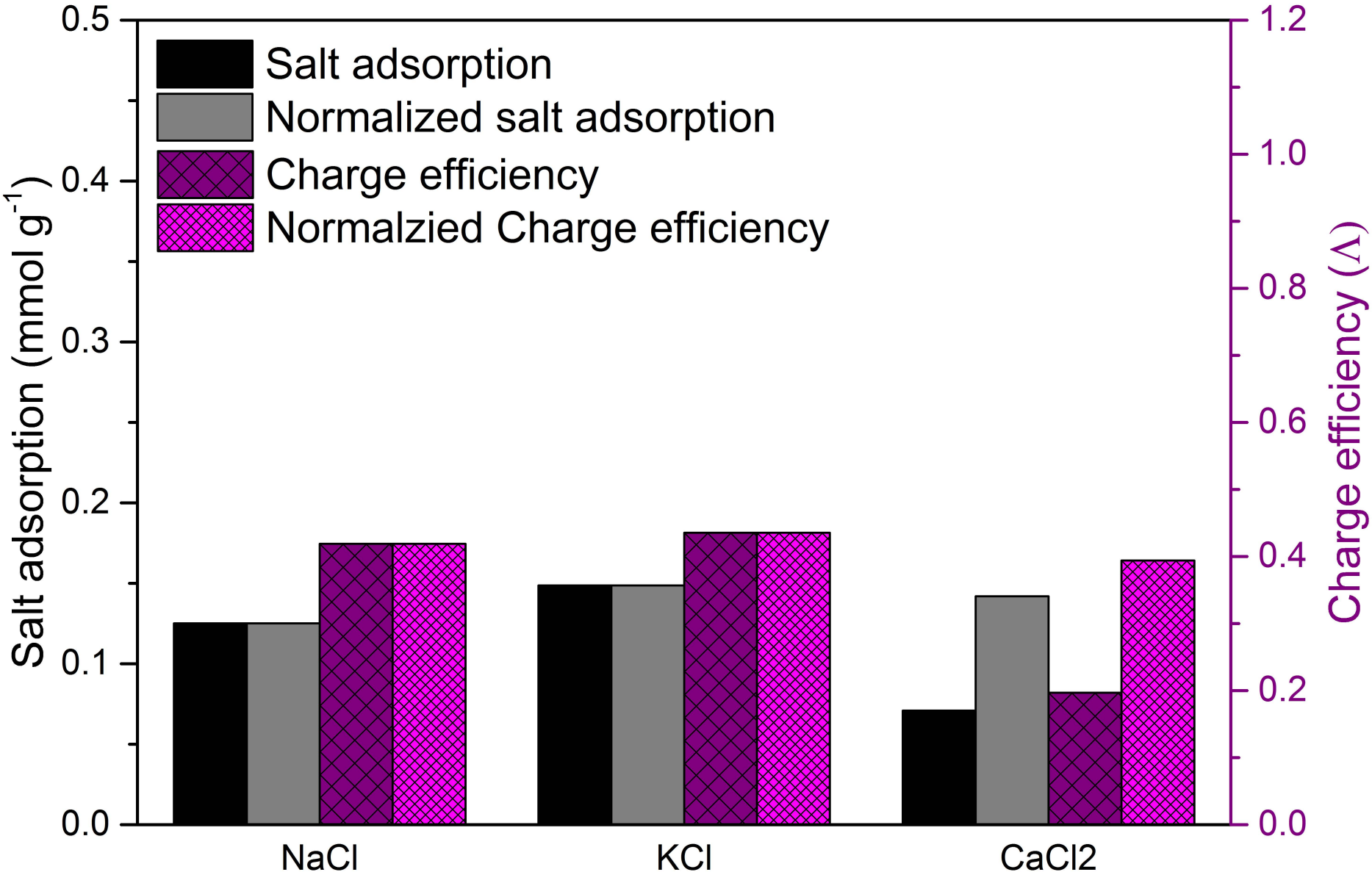
Salt adsorption
Normalized salt adsorption
Charge efficiency
Normalzied Charge efficiency
Salt adsorption (mmol g-1)
Charge efficiency (Λ)
0.0
0.1
0.2
0.3
0.4
0.5
0.0
0.2
0.4
0.6
0.8
1.0
1.2
NaCl
KCl
CaCl2

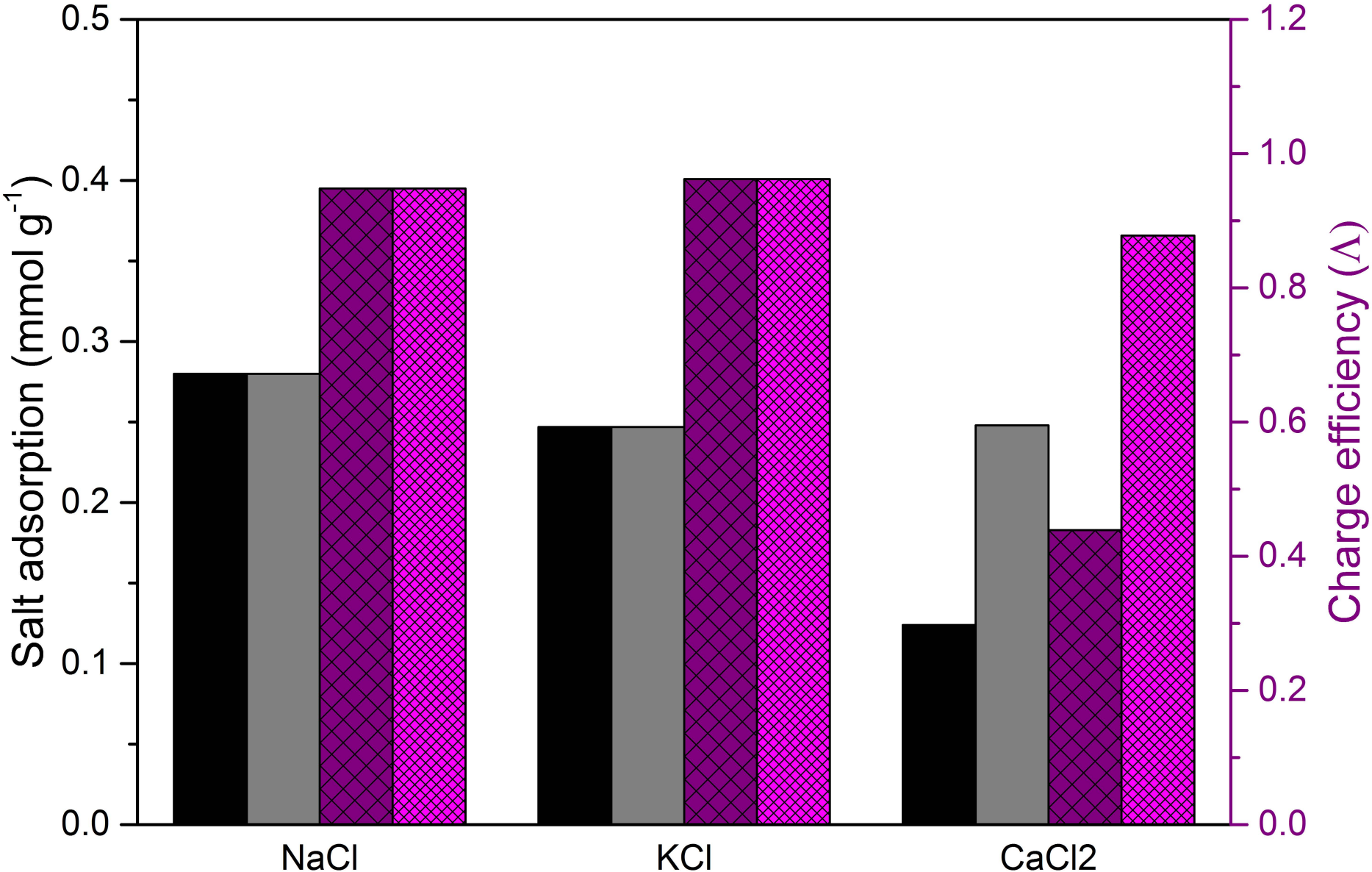
0.5
0.4
0.3
0.2
0.1
0.0
Salt adsorption (mmol g-1)
1.2
1.0
0.8
0.6
0.4
0.2
0.0
Charge efficiency (Λ)
NaCl
KCl
CaCl2

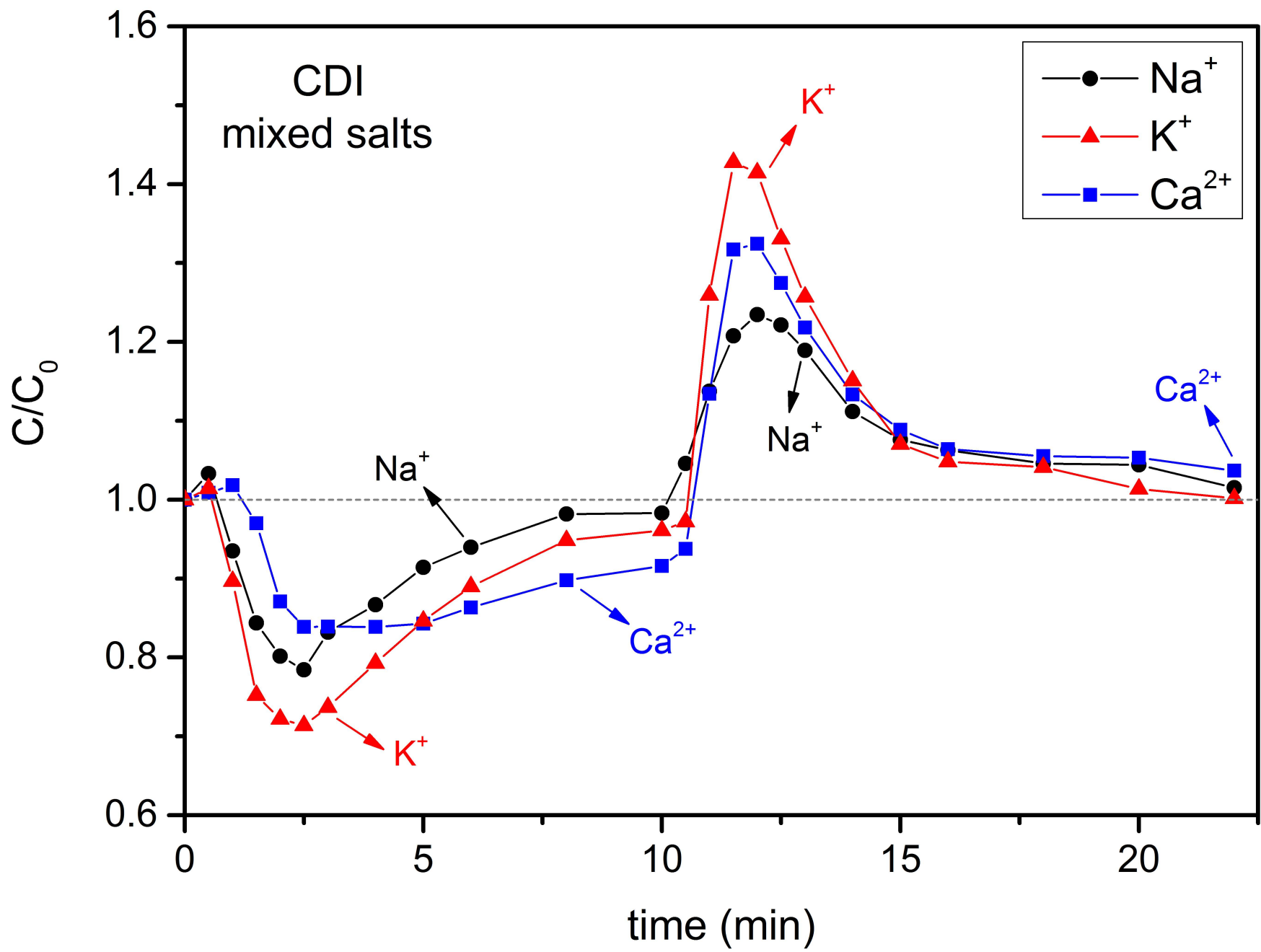
CDI
mixed salts
Na+
K+
Ca2+
C/C0
time (min)
1.6
1.4
1.2
1.0
0.8
0.6
0
5
10
15
20

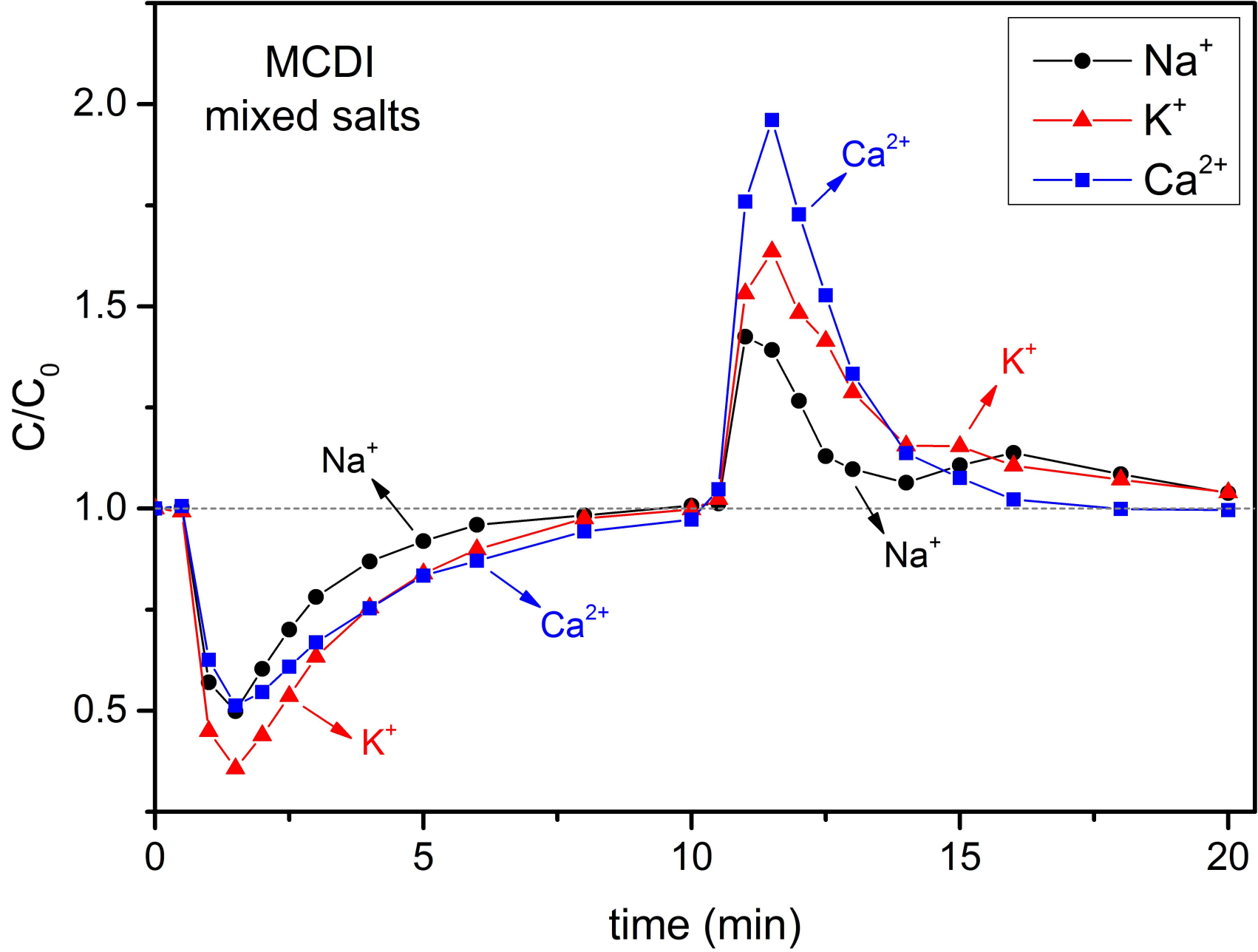
MCDI
mixed salts
Na+
K+
Ca2+
C/C0
time (min)
0
5
10
15
20
0.5
1.0
1.5
2.0

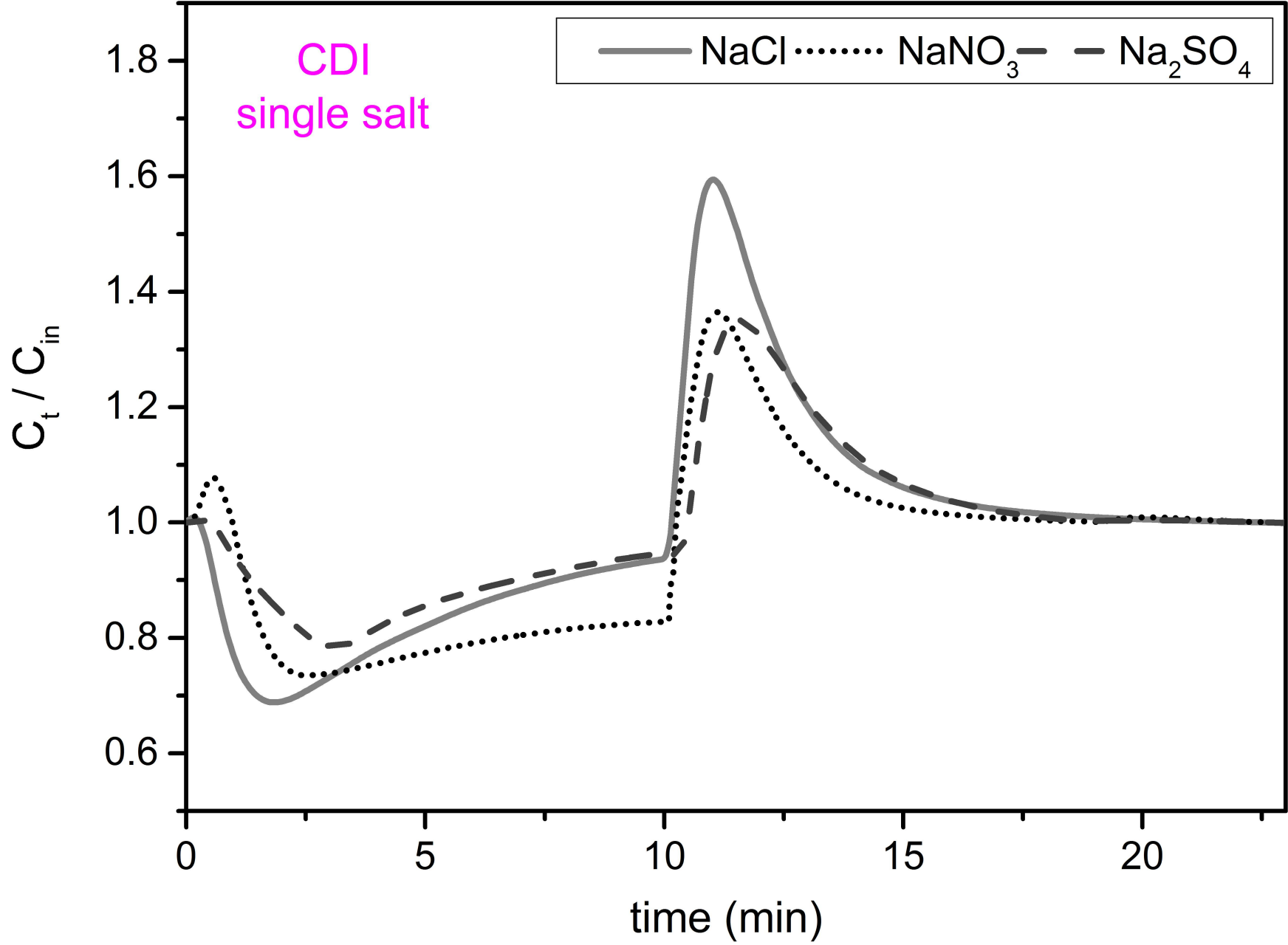
CDI
single salt
NaCl
NaNO3
Na2SO4
Ct / Cin
time (min)
1.8
1.6
1.4
1.2
1.0
0.8
0.6
0
5
10
15
20

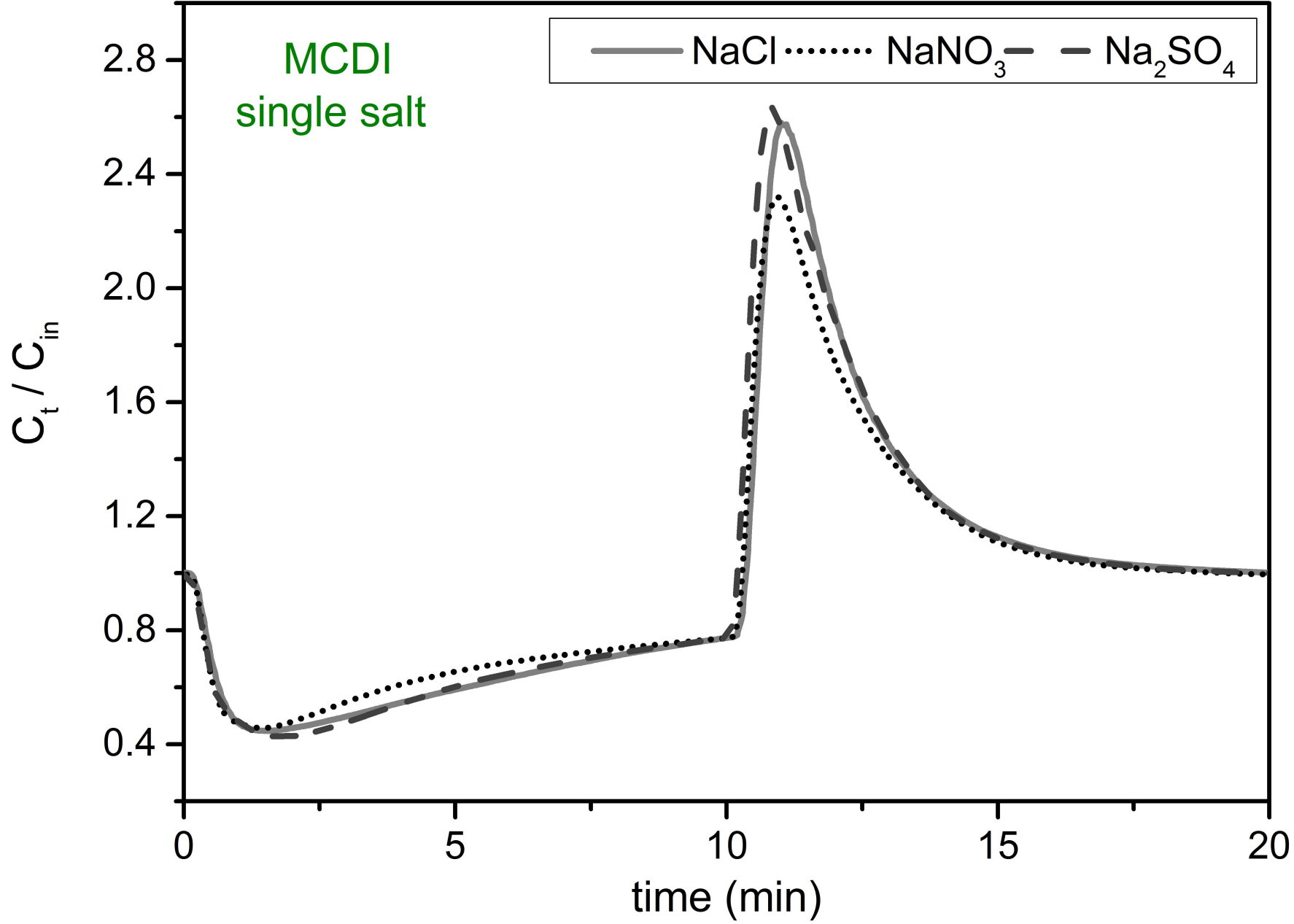
MCDI
single salt
NaCl
NaNO3
Na2SO4
Ct / Cin
time (min)
2.8
2.4
2.0
1.6
1.2
0.8
0.4
0
5
10
15
20

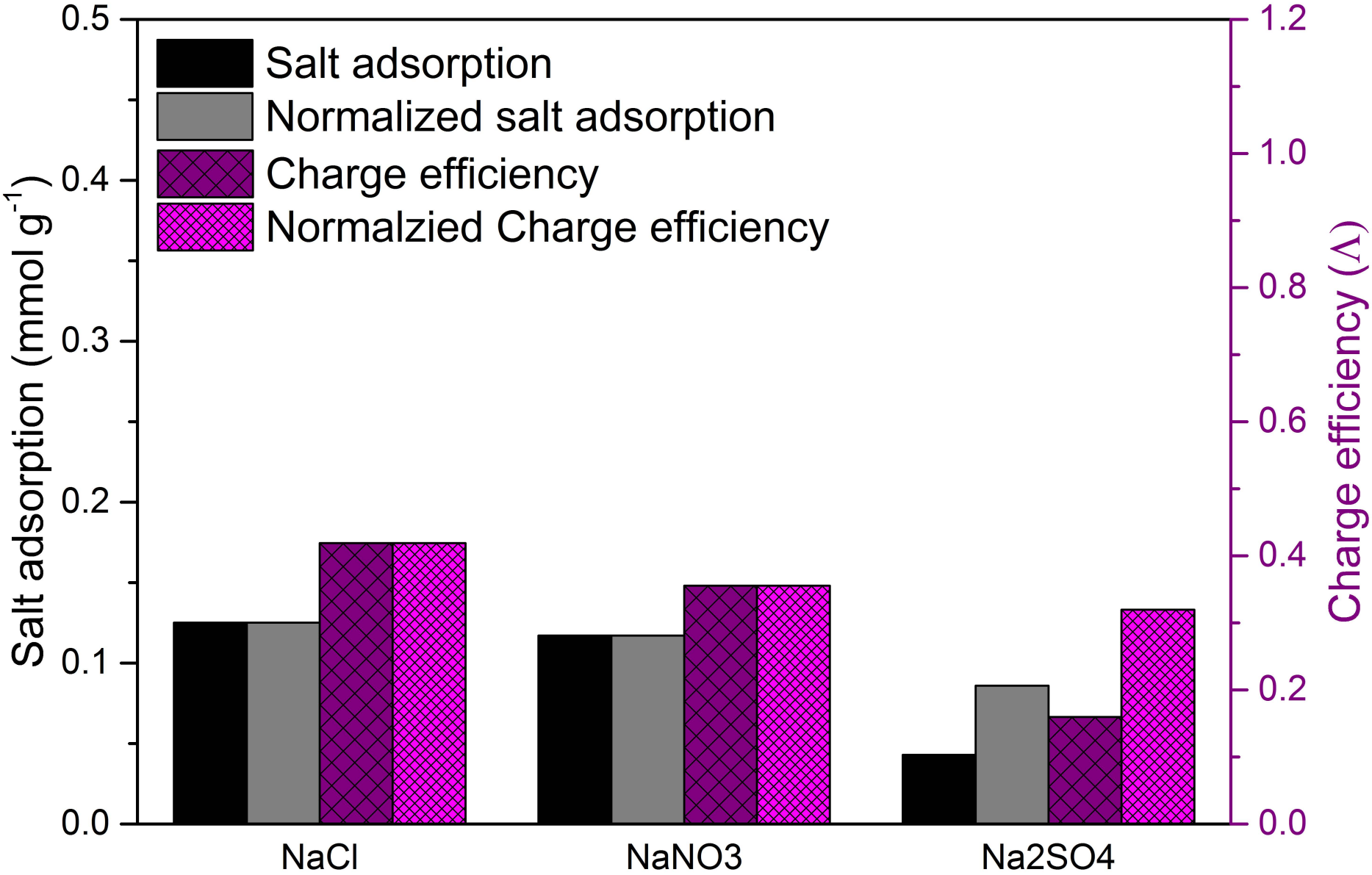
Salt adsorption
Normalized salt adsorption
Charge efficiency
Normalzied Charge efficiency
Salt adsorption (mmol g-1)
Charge efficiency (Λ)
0.0
0.1
0.2
0.3
0.4
0.5
0.0
0.2
0.4
0.6
0.8
1.0
1.2
NaCl
NaNO3
Na2SO4

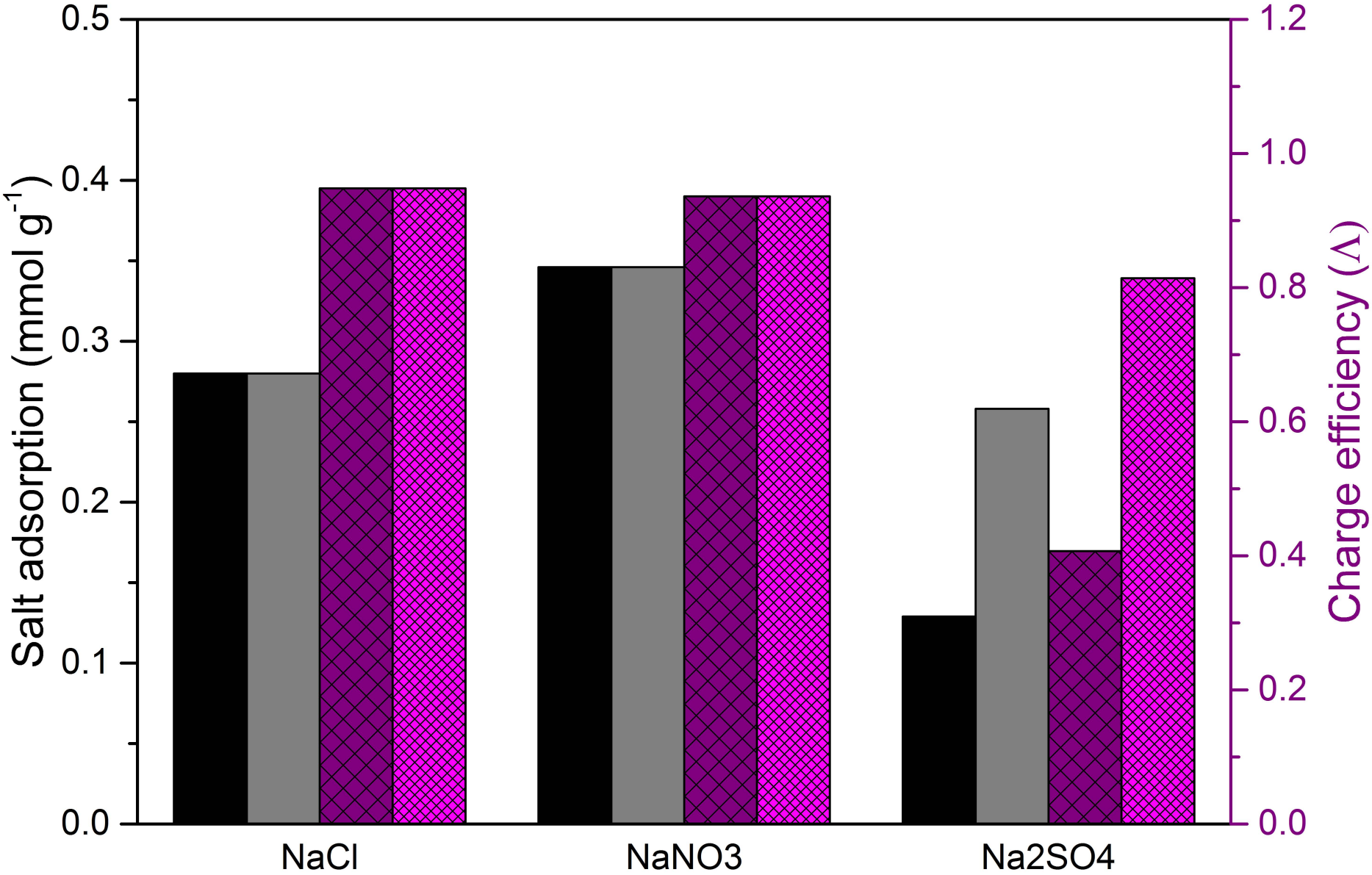
0.5
0.4
0.3
0.2
0.1
0.0
Salt adsorption (mmol g-1)
1.2
1.0
0.8
0.6
0.4
0.2
0.0
Charge efficiency (Λ)
NaCl
NaNO3
Na2SO4

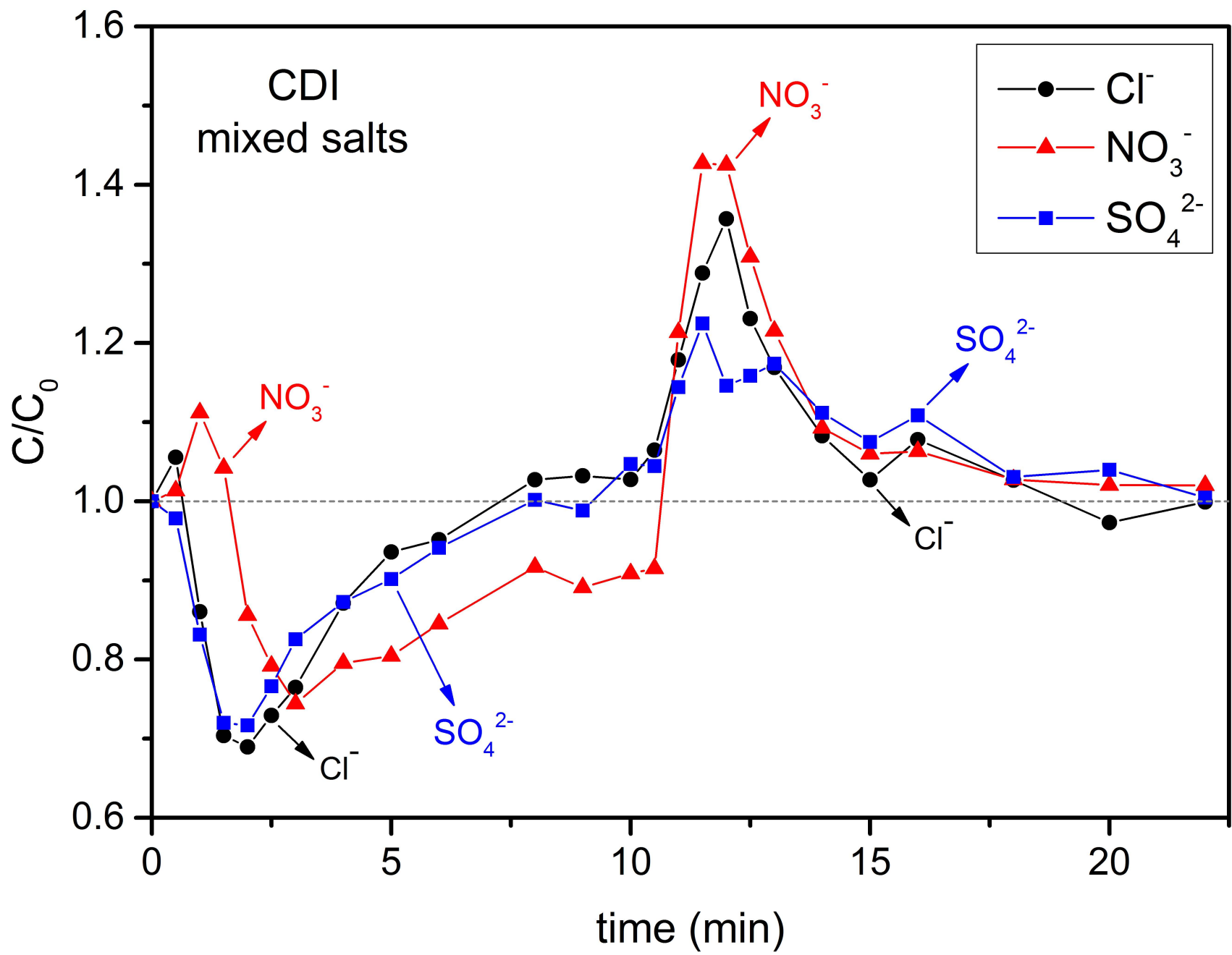
CDI
mixed salts
Cl-
NO3-
SO4 2-
C/C0
time (min)
1.6
1.4
1.2
1.0
0.8
0.6
0
5
10
15
20

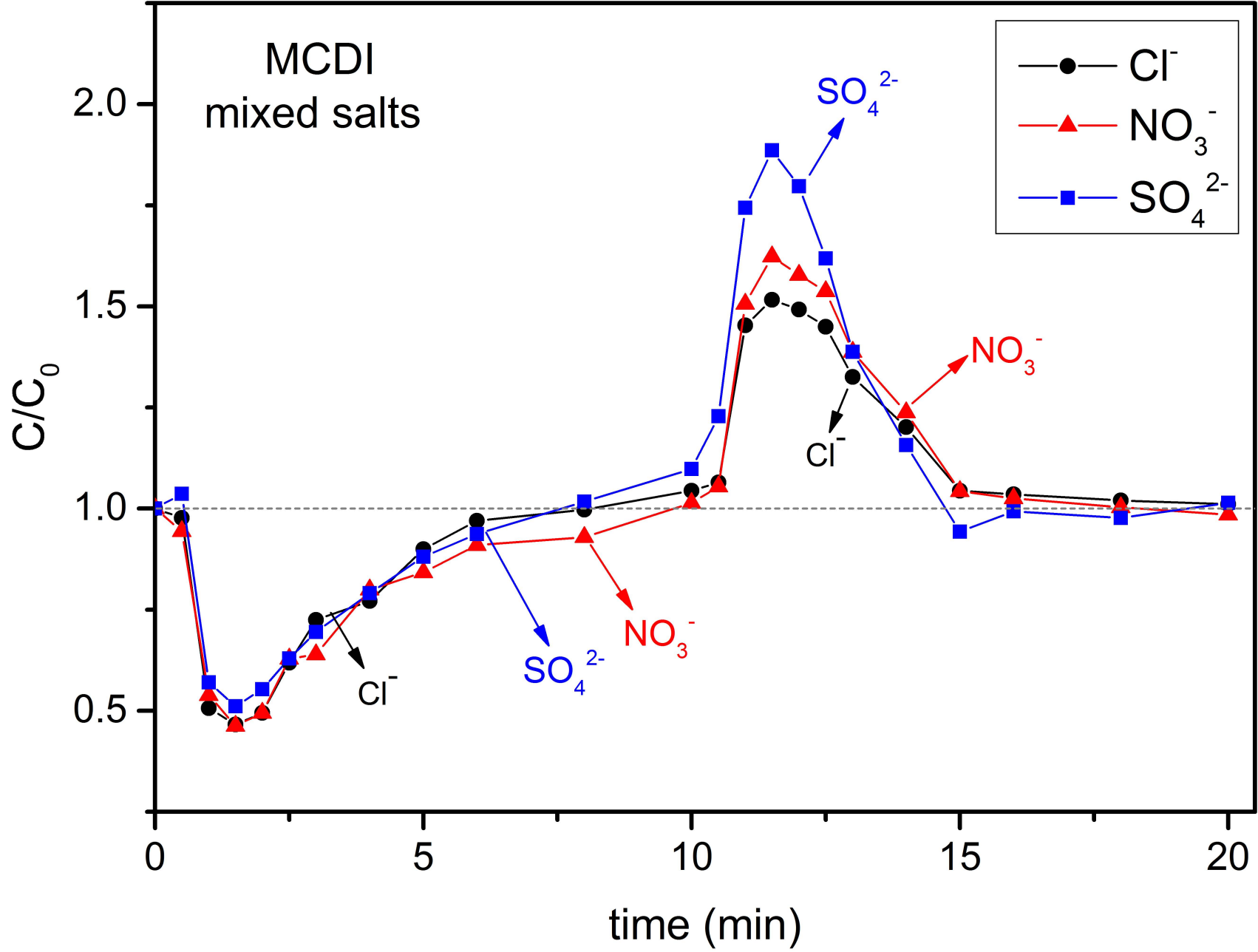
MCDI
mixed salts
Cl-
NO3-
SO4 2-
C/C0
time (min)
0
5
10
15
20
0.5
1.0
1.5
2.0

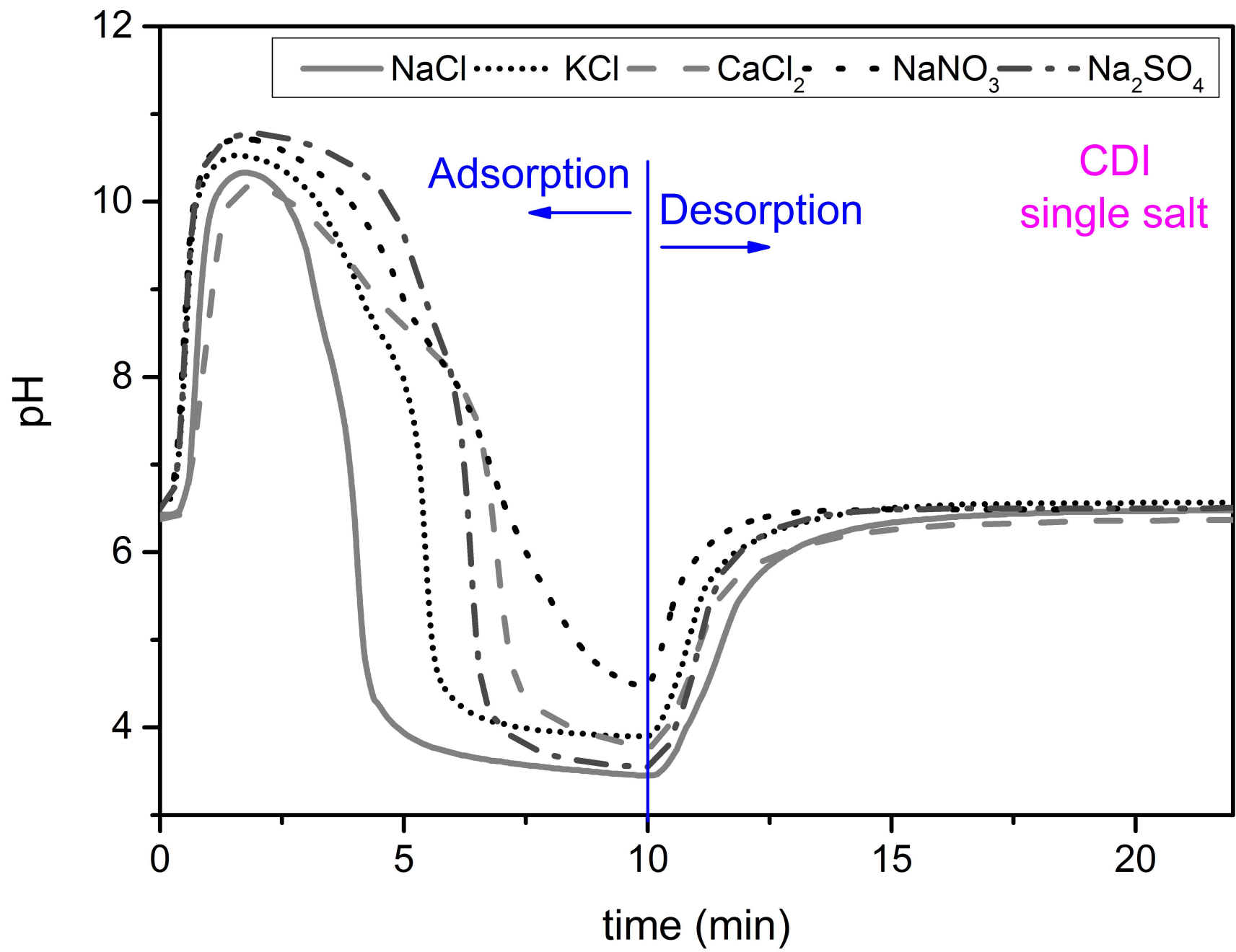
NaCl
KCl
CaCl2
NaNO3
Na2SO4
Adsorption
Desorption
CDI
single salt
pH
time (min)
12
10
8
6
4
0
5
10
15
20

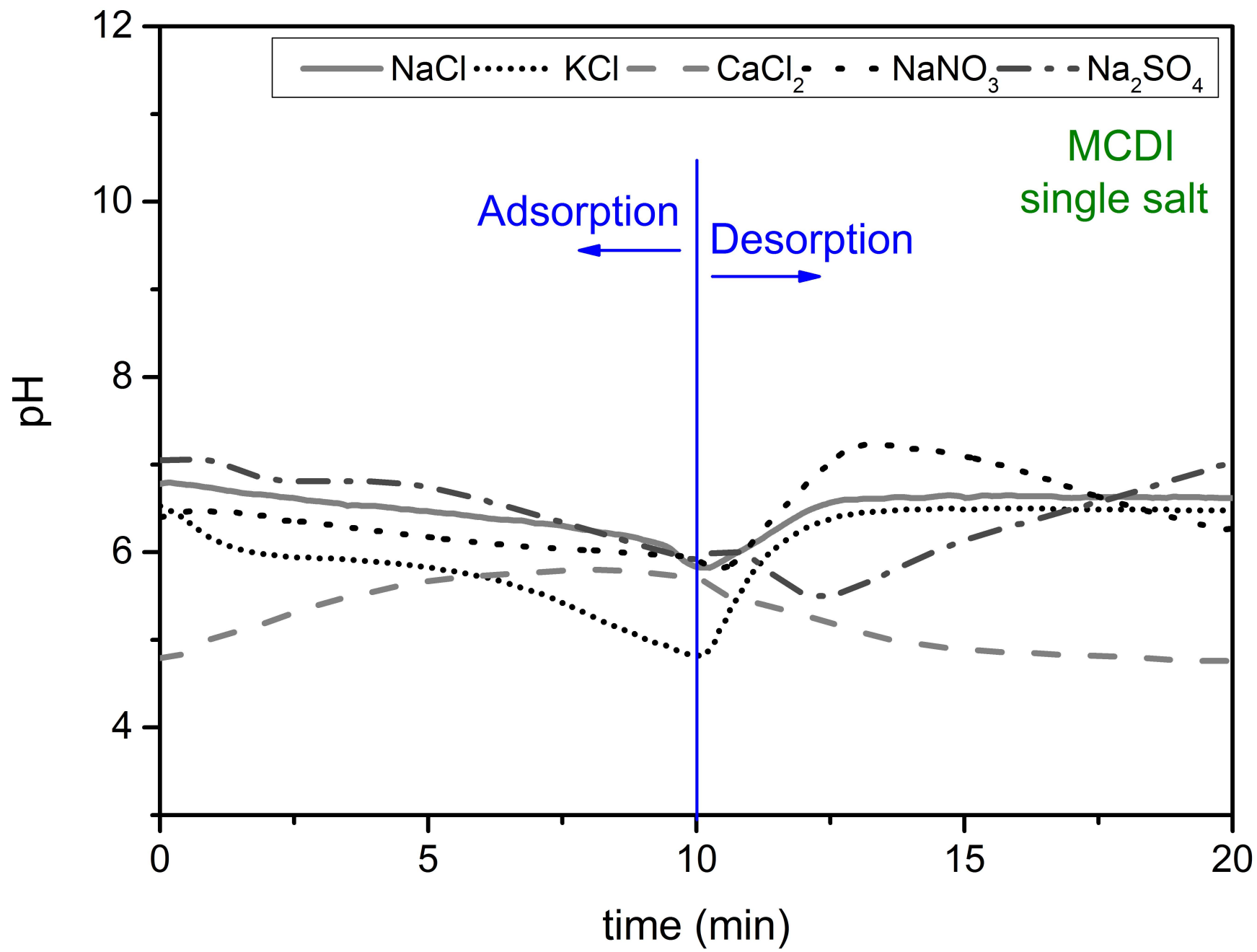
NaCl
KCl
CaCl2
NaNO3
Na2SO4
MCDI
single salt
Adsorption
Desorption
pH
time (min)
12
10
8
6
4
0
5
10
15
20